ELSEVIER

Dynamics of Atmospheres and Oceans 23 (1996) 155–169

dynamics of atmospheres and oceans

Energy dissipation and vortex structure in freely decaying, stratified grid turbulence

A.M. Fincham *, T. Maxworthy, G.R. Spedding

Department of Aerospace Engineering, University of Southern California, Los Angeles, CA 90089-1191, USA

Received 1 July 1994; revised 2 March 1995; accepted 6 March 1995

Abstract

Full field digital particle image velocimetry (DPIV) measurements of strongly stratified grid turbulence have been carried out for long times (up to $Nt \approx 1000$). Quasi-2D vortices were formed that were separated vertically by strong horizontal vortex sheets. Dissipation scales were resolved and the relative dissipation fractions in the horizontal and vertical planes were determined. A simple vortex model, involving a dense packing of discus-shaped structures connected by vortex lines that alternate between horizontal and vertical orientation, is shown to be consistent with both the observed velocity and vorticity fields, and the evolution of the measured length scales in orthogonal planes.

1. Introduction

In the low Froude number regime, one hypothesis for the approach to the final state of stratified turbulence characterizes it as a field of quasi-2D vortices, the members of which grow in time by pairing (see Maxworthy et al. (1987) and Yap and Van Atta (1993)). Many experiments (see the review by Hopfinger (1987)) have characterized the initial collapse and the statistical properties at early times. Numerical simulations by Riley et al. (1981), Lilly (1983), Metais and Herring (1989), and Lelong and Riley (1991) have examined the vertical structure, and the distribution of energy between wave and vortical modes. Experiments by Browand et al. (1987), and Liu et al. (1987) have provided information on the vertical spacing of these vortical structures. Such structures are thought to model those found in a stratified ocean, where they would be generated by mixing events covering a wide range of scales in both space and time. The present experiments

* Corresponding author.

SSDI 0377-0265(95)00415-7

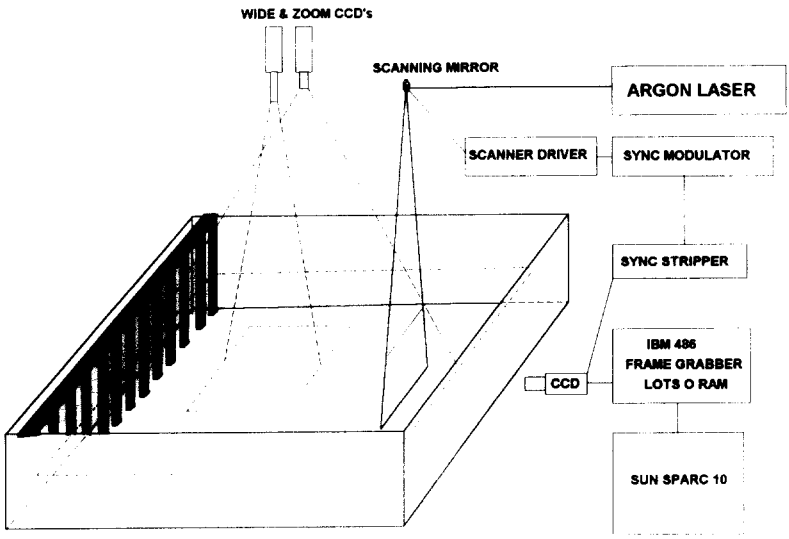

Fig. 1. Experimental configuration.

provide data for comparison with numerical simulations and oceanic observations, as well as for addressing the hitherto unanswered question concerning the importance of the vertical coupling between horizontal layers.

2. Experiments

The experiments were performed in a 2.4 m square tank that was linearly stratified to a depth of 15 cm with salt water. A rake of vertical flat-plates, of width $W = 3.8$ cm and mesh spacing $M = 15$ cm, was towed the full length of the tank. The vertical plates minimized internal wave generation and were chosen over rods as they provided a well-defined separation point, independent of the towing speed. Stepper motors drove both the rake and a profiling conductivity probe used to measure the density gradient before and after each run. The good repeatability attained by this automated set-up allowed the velocity fields in the horizontal and vertical planes to be measured in separate realizations of the same experiment. A high-resolution digital particle image velocimetry (DPIV) system was developed. This system was carefully optimized to maximize the measurable range of scales and velocities by using a combination of simulated and experimental flows. Under optimum conditions the measured mean r.m.s. error on velocity is less than 2% (Fincham and Spedding, 1995). Fig. 1 shows the experimental facility and the orientation of the measurement planes described below.

The measurements in the horizontal plane were made by densely seeding the central isopycnal with polystyrene beads of approximately 800μ diameter and density $1.0473 < \rho < 1.0477$ and lighting uniformly from above. This technique requires no light slice (or refractive index matching) and measurements of horizon-

tal velocity were obtained on an isopycnal surface. Two charged-couple device (CCD) cameras with different focal length lenses were synchronized in time to resolve simultaneously both the small dissipation scales and the larger flow features.

Vertical-plane measurements were made in a 20 cm × 15 cm rectangle located in the center of one end of the tank parallel to the rake. The fluid was seeded with micro-encapsulated rhodamine particles of approximately 50μ diameter. An oscillating mirror was phase locked to a single CCD camera and used to scan a thin vertical sheet of monochromatic laser light across the test area. This arrangement allowed effective pulsing of the light sheet without the complications associated with mechanical shuttering mechanisms.

Pairs of images were acquired direct to personal computer memory at 64 logarithmically spaced time steps over the typical 30 min duration of each experiment. Over 6000 images were processed using a 2D spatial cross-correlation to track groups of particles between image pairs. Each resulting velocity field was checked by eye and clearly erroneous vectors were removed before being fitted with a 2D smoothing spline (Spedding and Rignot, 1993) and spectrally 'flip-filtered' to remove grid scale fluctuations caused by pixel locking bias errors (Fincham and Spedding, 1995). Horizontal and vertical data planes were adjusted to a common origin in time based on the location of the rake, and statistical quantities could then be computed utilizing data from both planes. Owing to the discrete time sampling, it was often necessary to fit quantities from one plane with a continuous function of time so as to obtain values at times corresponding to measurements in the orthogonal plane.

Experiments were performed for towing speeds U, of 0.5, 1, 2, 4 and 8 cm s^{-1} and density gradients with buoyancy frequencies, N, of 1, 1.5 and 2 rad s^{-1}. The initial Reynolds number (Re_M) range based on the mesh spacing M, and Froude number (Fr) range, based on the bar width W, were $700 < Re_M < 12\,000$ and $0.1 < Fr < 2$.

3. Results and discussion

For a constant value of N, a noticeable change in horizontal and vertical structure was observed as the towing speed was increased. This was associated with the individual wakes of the rake bars undergoing a transition to turbulence. Even after long times these differences were still evident in both the vortex structure and the subtleties of the energy dissipation rates. A general description of the flow at low and high Reynolds number will be followed by a more detailed analysis of the viscous energy dissipation. Vortex interactions are then investigated with the help of a simple 3D vortex model.

3.1. General structure

At low Re_M [$O(10^3)$] a regular von Kármán type of vortex shedding was observed in the horizontal plane. The structures formed in this way immediately

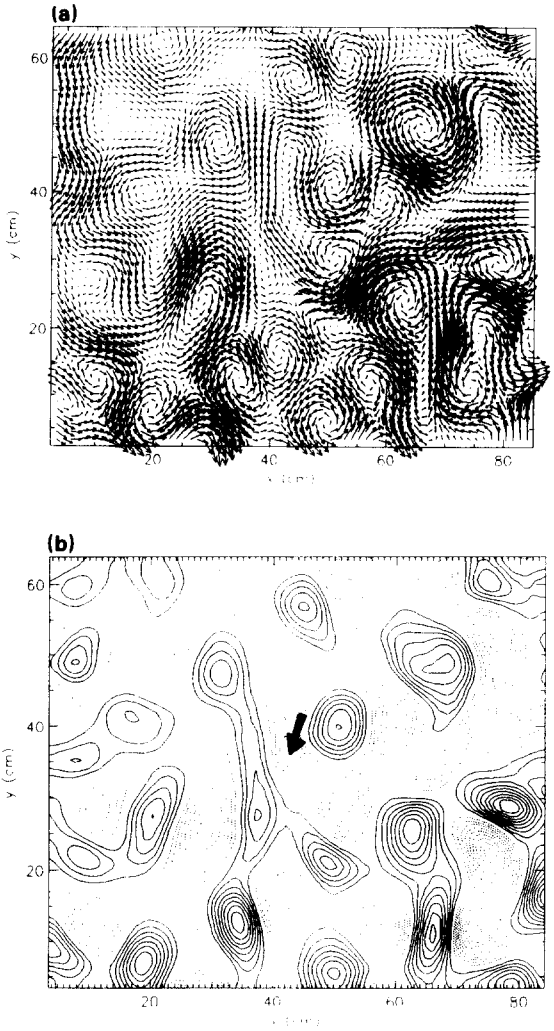

Fig. 2. ZOOM camera. $Re_M = 760$, $N = 2.3$, $t = 193$ s. grid was towed from top to bottom. (a) 2D velocity vector field $\boldsymbol{u}(x,y)$. (b) Computed vertical component of vorticity $\omega_z(x,y)$; the $\omega_z = 0$ contour line has been omitted and $\Delta\omega_z = 0.02\ s^{-1}$.

grouped together in a complex sea of opposite-signed vortices, as can be seen from the measurements of the close-up (ZOOM) camera above the tank (Fig. 2). The formation of dipole, quadrapole and hexapole structures is evident. Fig. 3 shows the view from the wide-angle (WIDE) camera, corresponding to the same time as Fig. 2. Comparison of the two shows some smaller vortex structures that are only resolved by the ZOOM camera (see arrow). There was an apparent transfer of energy to larger scales as vortices grew in time by pairing and diffusion until limited by the size of the tank.

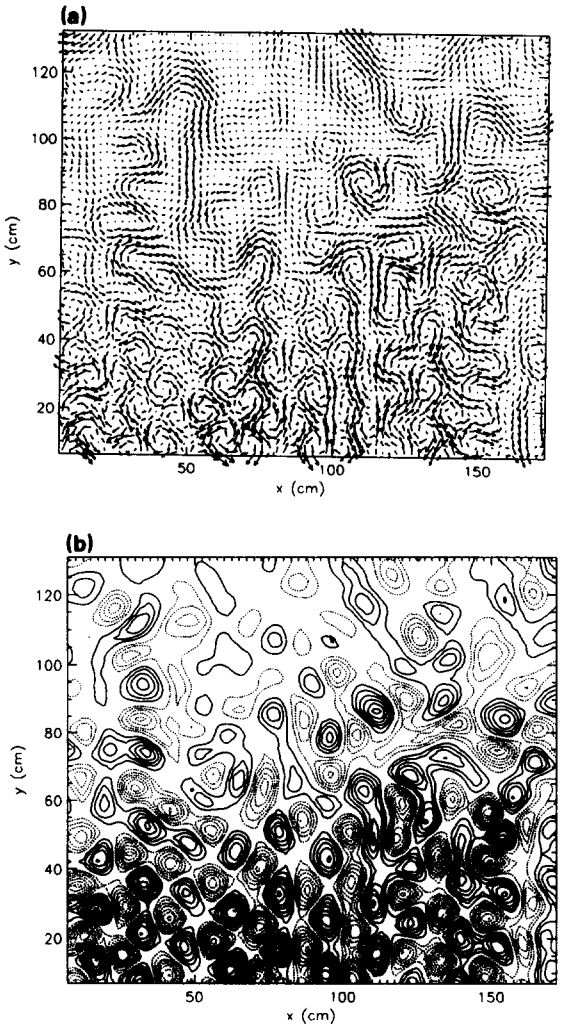

Fig. 3. WIDE camera view corresponding to same conditions as for Fig. 2. (a) $u(x,y)$. (b) $\omega_z(x,y)$, $\Delta\omega_z = 0.023\ s^{-1}$.

The shed vortices immediately de-correlate vertically, as indicated by the inflections in the vertical profiles of horizontal velocity in Fig. 4. The rake bar, centered in the test area, has just moved into the measurement plane 4 s earlier. The vertical coherence is lost as vortices are sheared apart producing multiple layers of eddies (Fig. 5). These layers are characterized by strong horizontal vorticity which has a sheet-like appearance, consisting of bands of alternating sign. Vertical interactions appeared to play a major role in the development of the flow, and specific instances of merging of like-signed vortex sheets were observed at all Reynolds numbers. At low speeds the vertical rake bars produced very small

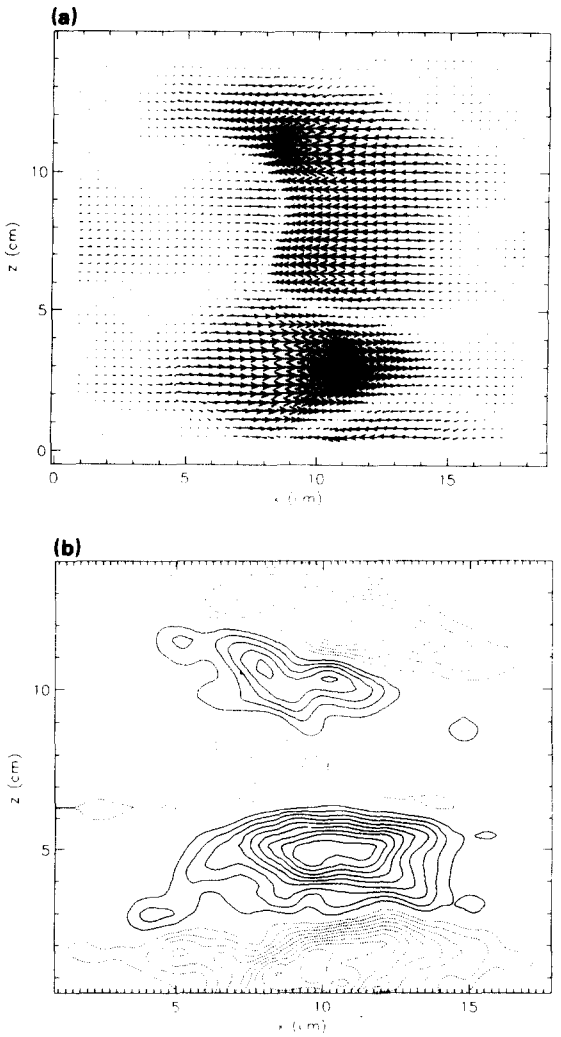

Fig. 4. Vertical section (VERT) directly behind rake bar, showing initial instability. $Re_M = 760$, $N = 2.38$, $t = 4$ s. (a) $\boldsymbol{u}(x,z)$. (b) $\omega_y(x,y)$, $\Delta\omega_y = 0.08$ s^{-1}.

vertical velocities, which were quickly damped by buoyancy forces, approaching zero (or the resolution of the measurement) after about 30 buoyancy periods.

At higher Re_M [$O(10^4)$] the flow was initially fully turbulent immediately behind the rake bars. Coherent horizontal structures with vertical vorticity emerged from the collapsing wakes, as the vertical velocity component was suppressed. Quasi-2D vortex pairings were accelerated owing to the shorter eddy turnover times and horizontal scales grew more quickly in time than in the low Re runs. The final state was often a single vortex, occupying the entire tank.

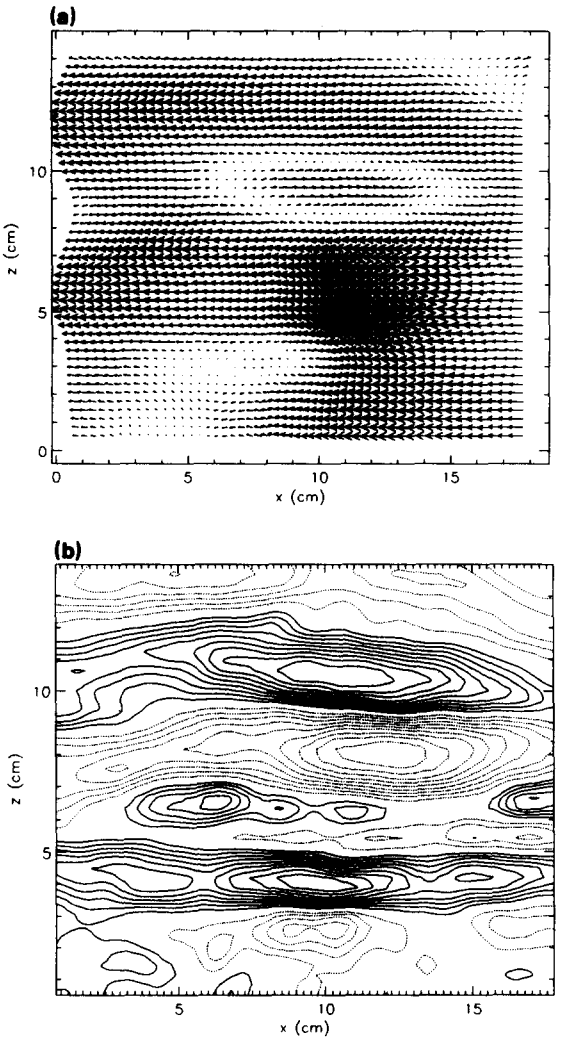

Fig. 5. VERT. $Re_M = 760$, $N = 2.38$, $t = 79$ s. (a) $u(x,z)$. (b). $\omega_y(x,y)$, $\Delta\omega_y = 0.025$ s^{-1}.

In the vertical plane, at early times the flow appears to be nearly isotropic, with strong overturning and large-amplitude internal waves. Nonetheless, layers formed, and appeared to thicken in time. Shearing between layers was stronger, and the horizontal r.m.s. vorticity, ω_y, was a factor of three times stronger than the vertical r.m.s. vorticity of the larger horizontal structures themselves, ω_z.

The formation of layers at these early times, when the flow is still energetic, produces strong shearing that cannot be stabilized by buoyancy forces. These shear layers are susceptible to Kelvin–Helmholtz-like instabilities, and vortex roll-up occurs, as shown in Fig. 6.

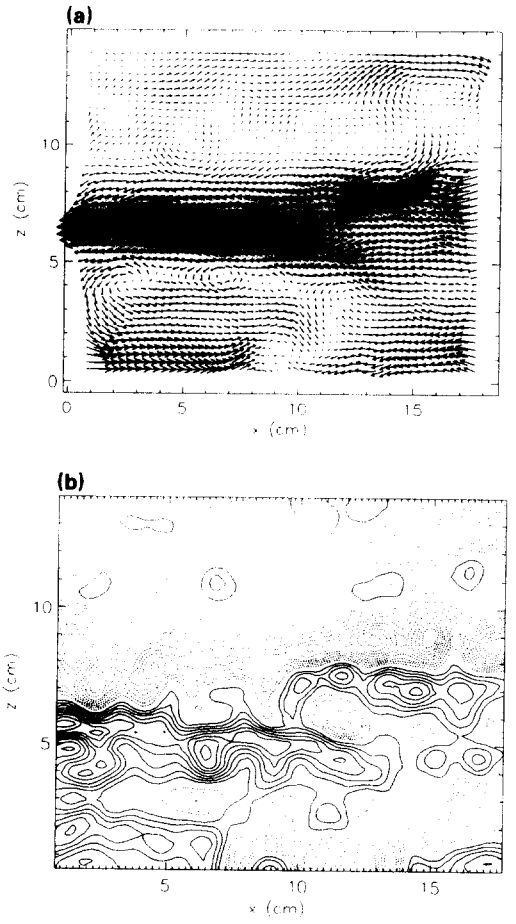

Fig. 6. VERT. $N = 2.3$ for $t = 29$ s. (a) $\boldsymbol{u}(x,z)$. (b) $\omega_y(x,y)$, $\Delta\omega_y = 0.25\ \mathrm{s}^{-1}$. Kelvin–Helmholtz-like roll up is evident at early times in the strongly stratified cases.

3.2. Kinetic energy decay

The mean kinetic energy is monitored in time by assuming homogeneity throughout the volume of the tank, and averaging the energy from the overhead cameras for each time step. The rate of decay of kinetic energy per unit volume, $\dot{E}$, can be determined from a power law fit of the $E(t)$ data from both the horizontal and vertical planes. In the weakly stratified case, early time decay rates varied from $t^{-1.4}$ to t^{-1} as $\mathrm{Re_M}$ was increased from 10^3 to 10^4. Fig. 7 shows the normalized decay for $N = 1.03$. This variation in decay rates is less pronounced in the stronger stratified runs.

Energy was lost primarily to viscous dissipation and a small increase in the mean potential energy owing to a buoyancy flux caused by small-scale vertical mixing.

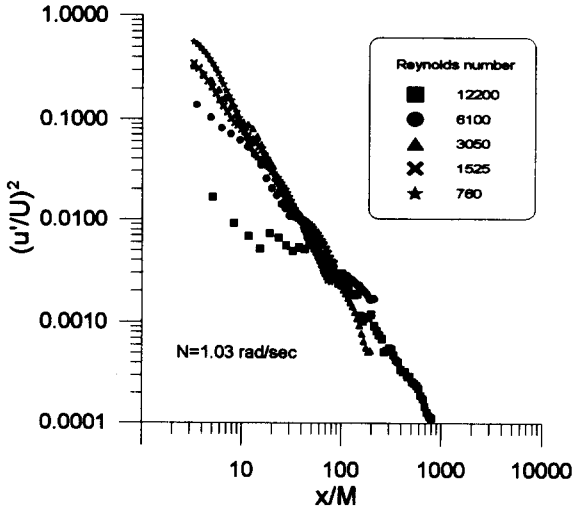

Fig. 7. Normalized energy decay for $N = 1.03$.

Park et al. (1994) measured mixing efficiencies for a stratified tank stirred by a single cylindrical rod, and extrapolating from their data, it is estimated that less than 5% of the kinetic energy input by the rake is used for mixing. This is also consistent with our own conductivity measurements. Furthermore, any such mixing will occur in the very early stages of the experiment right behind the grid, before the data acquisition process has started. Other losses owing to friction on the side walls and floor of the tank cannot be avoided but are believed to be small.

The total turbulent viscous dissipation per unit mass, ϵ_{tot} can be written as

$$\epsilon_{tot} = -2\nu\overline{s_{ij}s_{ij}} \tag{1}$$

where

$$s_{ij} = \frac{1}{2}\left(\frac{\partial u_i}{\partial x_j} + \frac{\partial u_j}{\partial x_i}\right), \quad i,j = 1,2,3$$

and ν is the kinematic viscosity.

Alternatively, expanding and dropping the − sign (Hinze, 1975, p. 72),

$$\epsilon_{tot} = \nu\overline{\frac{\partial u_j}{\partial x_i}\left(\frac{\partial u_i}{\partial x_j} + \frac{\partial u_j}{\partial x_i}\right)} \tag{2}$$

3.2.1. Dissipation in homogeneous isotropic turbulence

As DPIV methods typically provide two components of velocity in a plane, it is instructive to note how such planar measurements relate to the total dissipation in isotropic homogeneous turbulence. Stratified turbulence is not, of course, isotropic, but examination of the isotropic relations gives a useful reference point, and departures from this can be noted.

For isotropic homogeneous turbulence, there is no preferred spatial direction, and the dissipation can be expressed as

$$\epsilon_{tot} = 6\nu\left[\overline{\left(\frac{\partial u}{\partial x}\right)^2} + \overline{\left(\frac{\partial u}{\partial y}\right)^2} + \overline{\frac{\partial u}{\partial y}\frac{\partial v}{\partial x}}\right] \tag{3}$$

From continuity, and then following Taylor (1935),

$$\overline{\left(\frac{\partial u}{\partial x}\right)^2} + \overline{\left(\frac{\partial v}{\partial y}\right)^2} + \overline{\left(\frac{\partial w}{\partial z}\right)^2} = -2\left(\frac{\partial u}{\partial x}\frac{\partial v}{\partial y} + \frac{\partial v}{\partial y}\frac{\partial w}{\partial z} + \frac{\partial w}{\partial z}\frac{\partial u}{\partial x}\right) \tag{4}$$

Applying isotropy, and integrating the dissipation over a closed volume,

$$\overline{\left(\frac{\partial u}{\partial x}\right)^2} = -2\overline{\frac{\partial u}{\partial x}\frac{\partial v}{\partial y}} = -2\overline{\frac{\partial u}{\partial y}\frac{\partial v}{\partial x}} \tag{5}$$

Pure straining can eventually be related to simple shear by rotating the coordinate axis and applying isotropy to the resulting partial differential terms, hence

$$\overline{\left(\frac{\partial u}{\partial x}\right)^2} = \frac{1}{2}\overline{\left(\frac{\partial v}{\partial x}\right)^2} \tag{6}$$

Substituting (5) and (6) into (3), the total dissipation ϵ_{tot} can be expressed in terms of $\overline{(\partial u/\partial x)^2}$,

$$\epsilon_{tot} = 15\nu\overline{\left(\frac{\partial u}{\partial x}\right)^2} = 7.5\nu\overline{\left(\frac{\partial u}{\partial z}\right)^2} \tag{7}$$

Viscous dissipation owing solely to in-plane velocity gradients can be computed from the strain rate tensor in (1), where dissipation owing to gradients in a plane normal to the unit vector, $\hat{k}$ is given by

$$\epsilon_k = -2\nu\overline{s_{ij}s_{ij}} \quad i,j \neq k \tag{8}$$

So, dropping the $-$ sign,

$$\epsilon_z = 2\nu\left[\overline{\left(\frac{\partial u}{\partial x}\right)^2} + 2\overline{\left(\frac{\partial v}{\partial y}\right)^2} + \overline{\left(\frac{\partial u}{\partial y}\right)^2} + \overline{\left(\frac{\partial v}{\partial x}\right)^2} + 2\overline{\left(\frac{\partial u}{\partial y}\frac{\partial v}{\partial x}\right)}\right] \tag{9}$$

represents the contribution of velocity gradients in the horizontal plane to the total dissipation, or from isotropy, using (5) and (6)

$$\epsilon_z = 7\nu\overline{\left(\frac{\partial u}{\partial x}\right)^2} \tag{10}$$

So comparing (10) with (7), for isotropic homogeneous turbulence the in-plane velocity gradients will account for 7/15 of the total energy dissipation.

3.2.2. Dissipation measurements in stratified turbulence

In the stratified turbulence experiments the peaks in the dissipation spectra were fully resolved in both the horizontal and vertical planes, implying that all the dissipation scales are accounted for. All components of the deformation tensor are measured, but some of the cross-straining terms associated with Eq. (5) can only be estimated, as the measurements in orthogonal planes were not made simultaneously. However, owing to the dominance of the vertical shearing term $\overline{(\partial u/\partial x)^2}$ (recall the relative strengths of ω_z and ω_y) these cross straining terms are relatively unimportant in affecting the late time global energy decay rates.

In-plane dissipations ϵ_y and ϵ_z were computed from (8) for various Reynolds numbers. Owing to isotropy in the horizontal plane $\epsilon_x = \epsilon_y$ and the total viscous dissipation ϵ_{tot} can be expressed as

$$\epsilon_{tot} = \epsilon_z + 2\epsilon_y - 2\nu\left[\overline{\left(\frac{\partial u}{\partial x}\right)^2} + \overline{\left(\frac{\partial v}{\partial y}\right)^2} + \overline{\left(\frac{\partial w}{\partial z}\right)^2}\right] \tag{11}$$

Fig. 8 shows the contributions to the total dissipation $\dot{E}$ (continuous line) from gradients in the horizontal plane ϵ_z (triangles). At low $\mathrm{Re_M}$, ϵ_z accounts for slightly over 20% of the total energy decay, but this fraction is quickly reduced to less than 5% with increasing $\mathrm{Re_M}$. For higher Reynolds numbers, further reduction of the contribution of the horizontal velocity gradients to the total dissipation is evident (compare Figs. 8(a) and 8(b)). Vertical shearing increases, and $\overline{(\partial u/\partial z)^2}$ and $\overline{(\partial v/\partial z)^2}$ dominate the vertical plane dissipation and account for over 90% of ϵ_{tot}

$$\epsilon_{tot} \approx 2\epsilon_y \approx 2\nu\overline{\left(\frac{\partial u}{\partial z}\right)^2} \approx \dot{E} \tag{12}$$

as indicated in Fig. 8, where vertical gradient terms (star symbols) by themselves are good approximators of the total energy decay $\dot{E}$. It should be noted that, comparing (12) and (7), the assumption of isotropy for this flow leads to a 375% error in the dissipation rate ϵ_{tot}.

The importance of vertical shearing in the dissipation budget was first realized by Lilly (1983), using the wave vortex mode decomposition of Riley et al. (1981). Lilly obtained equations for 2D nonlinear flow with vertical structure (termed stratified turbulence equations by Lilly), and pointed out that independently evolving horizontal layers will quickly decorrelate vertically producing large vertical shearing and 3D turbulence, not accounted for in the theory. Metais and Herring (1989) conjectured that Lilly's stratified turbulence is plausible if vertical shear stabilized by buoyancy forces removes the energy. Yap and Van Atta (1993) measured the horizontal velocity field at a strongly stratified interface and found that the horizontal velocity gradients accounted for only a small fraction of the total energy decay. They inferred that this was due to strong velocity gradients between the fluid motion in the interface and the unstratified layers above and below it. Fincham et al. (1992, 1993) also made similar measurements for a

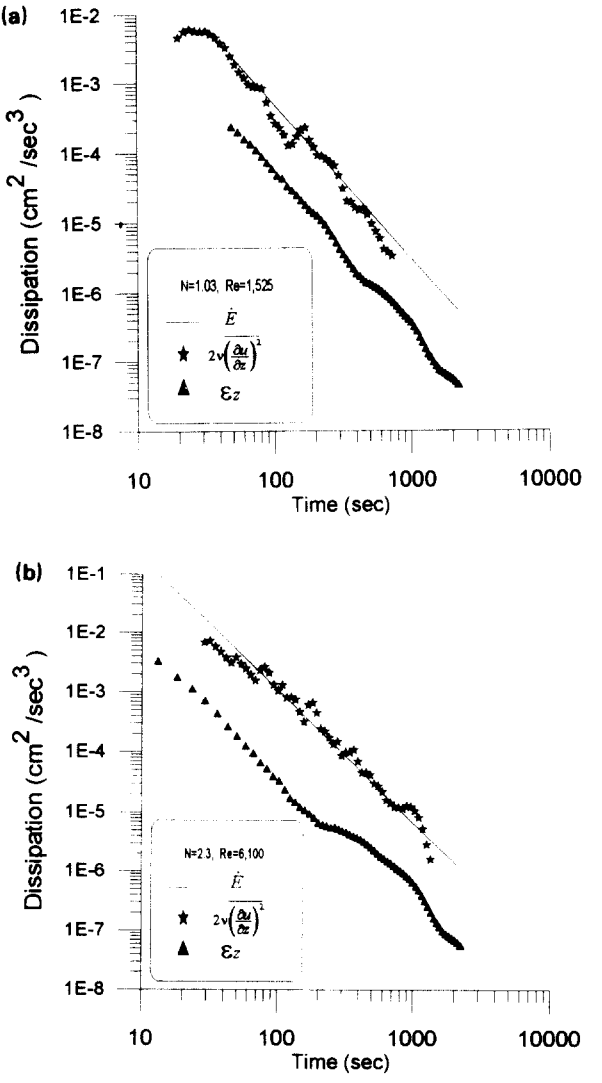

Fig. 8. Total energy decay rate $\dot{E}$, horizontal-plane dissipation ϵ_z, and $2\nu\overline{(\partial u/\partial z)^2}$ vs. time for (a). $\mathrm{Re_M} = 1525$, $N = 1.03$ rads^{-1}. (b) $\mathrm{Re_M} = 6100$, $N = 2.3$ rads^{-1}. The total energy decay $\dot{E}$ can be accurately approximated by $2\nu\overline{(\partial u/\partial z)^2}$ in both cases.

two-layer stratification, but concluded that the effects of stratification could not easily be isolated, owing to the potential for energy transfer between the thin stratified layer and the relatively thick layers of homogeneous fluid on either side. Here, in turbulence occurring within a linear density gradient, it is clear that the formation and subsequent interaction between neighboring layers throughout the depth is primarily responsible for the overwhelming majority of the dissipation of kinetic energy.

3.3. Vortex structures

Quasi-2D vortex pairings between eddy structures at slightly vertical locations forces the creation of strong shearing regions, and is probably responsible for initial layer development. Vertical coherence is lost, generating high shear regions as counter-rotating structures are forced to move over one another.

Horizontal length scales were computed from the integral of the longitudinal two-point velocity correlation function applied to the WIDE camera data. This integral scale L_h was found to agree with a mean vortex diameter, D, computed from a vortex counting algorithm. The growth of this integral scale with x/M initially collapsed for all Reynolds numbers. This collapse indicates that the scale is initially growing by a nonlinear vortex pairing mechanism, and so the growth rate should be determined by horizontal eddy turnover times.

Vertical, transverse two-point velocity correlations indicated a vertical scale corresponding to a mean spacing of like-signed bands of vorticity, and is equated to the vortex structure thickness, L_v. Owing to the small sampling area of the vertical light sheet, the determination of this vertical scale was noisy, but within these limits it agreed fairly well with that obtained from a manual counting method. Initial L_v shows a decrease related to the formation of the layers, followed by some equilibrium stage, after which the scale grows until limited by the depth of the tank. This vertical scale L_v shows no collapse with x/M and appears to grow in a somewhat diffusive manner at late times. A more detailed discussion of the temporal evolution of these length scales, along with their sensitivity to changes in Reynolds number and Froude number, will be published elsewhere.

In these types of flow it appears that the energy is contained in oblate-spheroidal or discus-shaped structures, but is being dissipated in thin horizontal shear layers at their borders. In section, each discus structure corresponds to a blob of vertical vorticity bound on either side by two opposite-signed, horizontal vortex sheets. An example of a cross-section of this type of structure is seen in Fig. 5, and a sketch is shown in Fig. 9.

The smoothness of the vorticity fields, which were measured at arbitrary planes, indicates a continuum of structures that densely fill the volume. This suggests a dense vortex packing in which vortex lines can connect a number of structures, as they meander through the fluid and eventually form closed vortex loops. Vertical vorticity is bent horizontally in the high shear regions, and these dissipative vortex sheets can then connect with neighboring structures on either side (see Fig. 10).

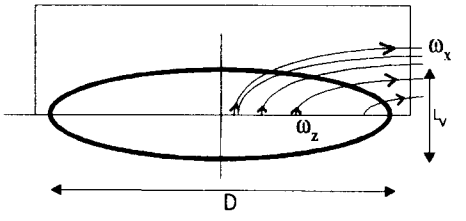

Fig. 9. Schematic diagram of single discus vortex showing vortex lines and length scales.

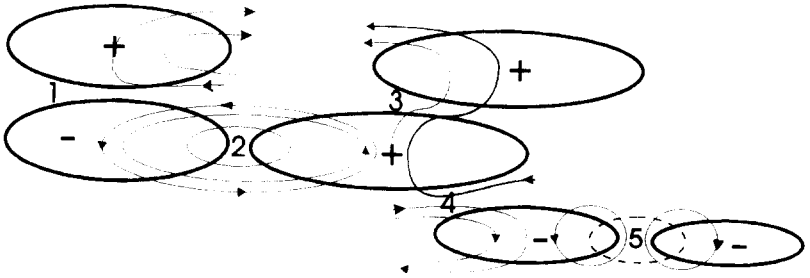

Fig. 10. Cross-sectional schematic diagram of possible vortex line connections between structures. The plus and minus signs indicate the direction of the vertical component of vorticity, ω_z. The Type 2 connection can be identified as a vortex dipole, and Type 3 is the most commonly observed; Type 5 indicates that two like-signed vortices require a third vortex of opposite ω_z in order to be interconnected on the same level. Connections of Type 1 and 4 are not commonly realized and may be unstable.

This tendency for vortex lines to connect to adjacent structures helps explain why we do not observe the strong, isolated vortices often found in numerical simulations of 2D turbulence (e.g. McWilliams, 1984).

4. Conclusions

The hypothesized two-dimensionality of collapsed stratified flows has been re-examined in the light of the observation that strong vertical shearing exists between horizontal layers, and the requirement that vortex lines form closed loops. This suggests a complex 3D network of structures in which layers of eddies cannot evolve independently of one another. The velocity fields generated by the simulations of Metais and Herring (1989) (see their Fig. 22(b)) in which the flow is initially dominated by the vortical component, have some qualitative similarities to our measurements, and a more detailed comparison involving 3D eddy structures themselves should be made. No attempt has been made here to decouple wave and vortex modes. As we believe that meso-scale eddies in the ocean and stratosphere exhibit similar interactions to those observed here, such measurements can be used to identify the location and dynamics of these dominant, local sources of energy dissipation.

Acknowledgments

We gratefully acknowledge support from the Office of Naval Research Fluid Mechanics Program under Contract NOOO14-J-92-1062.

References

Browand, F.K., Guyomar, D. and Yoon, S.C., 1987. The behavior of a turbulent front in a stratified fluid. J. Geophys. Res., 92: 5427–5433.

Fincham, A.M. and Spedding, G.R., 1995. Low cost high resolution DPIV for turbulent flows. Exp. Fluids, in preparation.

Fincham, A.M., Spedding, G.R., Maxworthy, T. and Browand, F.K., 1992. Turbulence and wakes, experiments in a stratified fluid. Bull. Am. Phys. Soc., 37(8): 1805.

Fincham, A.M., Spedding, G.R. and Maxworthy T., 1993. The horizontal and vertical structure of the vorticity field in freely decaying stratified grid turbulence. Bull. Am. Phys. Soc., 38(12): 2254.

Hinze, J.O., 1975. Turbulence. McGraw–Hill, New York.

Hopfinger, E.J., 1987. Turbulence in stratified fluids: a review. J. Geophys. Res., 92: 5287–5303.

Lelong, M.P. and Riley, J.J., 1991. Internal wave–vortical interactions in strongly stratified flows. J. Fluid Mech., 232: 1–19.

Lilly, D.K., 1983. Stratified turbulence and the meso-scale variability of the atmosphere. J. Atmos. Sci., 40: 749–761.

Liu, Y.N., Maxworthy, T. and Spedding, G.R., 1987. Collapse of a turbulent front in a stratified fluid. J. Geophys. Res., 92: 5427–5433.

Maxworthy, T., Caperan, P. and Spedding, G.R., 1987. The kinematics of quasi-2D, freely decaying turbulence in a stratified fluid. Third Int. Symp. on Strat. Flows, Pasadena, CA, February 1987. California Institute of Technology, Pasadena, CA.

McWilliams, J., 1984. The emergence of isolated coherent vortices in turbulent flow. J. Fluid Mech., 146: 21–43.

Metais, O. and Herring, J.R., 1989. Numerical simulations of freely evolving turbulence in stably stratified fluids. J. Fluid Mech., 202: 117–148.

Park, Y.-G., Whitehead, J.A. and Ghanadeskian, A., 1994. Turbulent mixing in stratified fluids: layer formation and energetics. J. Fluid Mech., 279: 279–311.

Riley, J.J., Metcalfe, R.W. and Weissman, M.A., 1981. Direct numerical simulations of homogeneous turbulence in density stratified fluids. In: B.J. West (Editor), Proc. AIP Conf. Nonlinear Properties of Internal Waves, 1981. American Institute of Physics, New York, pp. 79–112

Spedding, G.R. and Rignot, E.J.M., 1993. Performance analysis and application of grid interpolation techniques for fluid flows. Exp. Fluids, 15: 417–430.

Taylor, G.I., 1935. Statistical theory of turbulence, part 1. Proc. R. Soc. London, Ser. A, 151: 421–444.

Yap, C.T. and van Atta, C.W., 1993. Experimental studies of the development of quasi-2-dimensional turbulence in a stably stratified fluid. Dyn. Atmos. Oceans, 19: 289–323.